


## RESEARCH ARTICLE

# Investigation of wind load on 1,000 m-high super-tall buildings based on HFFB tests

Bo Li<sup>1,3</sup>  | Qingshan Yang<sup>2,3</sup> | Giovanni Solari<sup>4</sup> | Di Wu<sup>1,3</sup>

<sup>1</sup>School of Civil Engineering, Beijing Jiaotong University, Beijing 100044, China

<sup>2</sup>School of Civil Engineering, Chongqing University, Chongqing 400044, China

<sup>3</sup>Beijing's Key Laboratory of Structural Wind Engineering and Urban Wind Environment, Beijing 100044, China

<sup>4</sup>Department of Civil, Chemical and Environment Engineering, Polytechnic School, University of Genoa, Genoa 16145, Italy

## Correspondence

Bo Li, School of Civil Engineering, Beijing's Key Laboratory of Structural Wind Engineering and Urban Wind Environment, Beijing Jiaotong University, Beijing 100044, China.  
Email: libo\_77@163.com

## Funding information

National Natural Science Foundation of China, Grant/Award Number: 51378060 and 91215302; 111 Project of China, Grant/Award Number: B13002

## Summary

This paper studies the wind load on 1,000 m-high super-tall buildings and provides basic reference for design, including the utilization of passive and active control devices. High-frequency force balance wind tunnel tests of super-tall buildings with different height are carried out to investigate the effects of building height and wind flow on the wind load. Both monsoon and typhoon climate wind flows are simulated based on target models suggested in literatures. The simulation of typhoon climate wind flows is carried out by a newly developed technique. The analysis of the experimental results confirms that the aerodynamic force is very sensitive to both building height and wind flow. In monsoon climate, the turbulence intensity decreases on increasing the height above ground. Thus, on increasing the building height, vortex shedding becomes increasingly intense and excites stronger structural vibrations in the across-wind direction, though the across-wind fluctuating overturning moment coefficient is almost the same. In typhoon climate, both the mean and the fluctuating overturning moment coefficients increase with the building height. This is mainly caused by the decreasing mean wind speed. The vortex excitation becomes weaker on increasing the building height, and this phenomenon is different from that observed in the monsoon climate. In order to better explain vortex-shedding excitation, a new parameter referred to as the characteristic turbulence intensity is defined herein as a weighted mean value of the turbulence intensity in the range of the building height. It provides a robust interpretation of the vortex excitation of super-tall buildings located in different wind flow and climate conditions.

## KEYWORDS

1,000 m-high super-tall building, across-wind load, along-wind load, monsoon, typhoon, wind tunnel tests

## 1 | INTRODUCTION

In the recent boom of super-tall buildings, the structural height is becoming taller and taller with new construction. The tallest building in the world, Burj Khalifa, reaches 828 m. The tallest building under construction, Kingdom Tower, even reaches 1,000 m high. The new projects of the Dubai Observation Tower and Next Tokyo involve heights widely in excess of 1,000 m.<sup>[1]</sup> The need for super-tall buildings in China has been increasing with the fast-growing economy. According

to the database of the Council on Tall Buildings and Urban Habitat, in the world, there are 17 buildings completed or under construction with height beyond 500 m, and 10 of them are located in China (Table 1). According to a later survey,<sup>[2]</sup> in China, there are 35 super-tall buildings with height exceeding 500 m completed or under construction or under design. It is foreseen that the construction of 1,000 m-high buildings is not too far away in the future of China.

New material and construction techniques help to increase the height of buildings, but they result in more and more flexible structural systems, which are very sensitive to wind loads. Thus, safety, comfort, and control techniques under wind actions become key factors<sup>[3]</sup> in the structural design of these buildings.

After nearly half century of continuous investigations, the wind-resisting behavior of tall buildings is now relatively clear with reference to aerodynamic wind loading, wind-induced responses, aeroelastic effects, equivalent static wind loads, and control methods.<sup>[4–21]</sup> However, when the height of buildings is close to 1,000 m, many new problems arise that include the wind-flow representation, the aerodynamic, and aeroelastic performances. In particular, 1,000 m-high super-tall buildings may fall victims of excessive levels of vibration under the action of wind, adversely affecting serviceability and occupant comfort. To ensure their functional performance, various design interventions are necessary, ranging from alternative structural systems to the utilization of passive and active control devices.<sup>[17]</sup> This is a big challenge for researchers and engineers.

It is usually believed that, for a given terrain roughness or wind profile, the aerodynamic wind load on tall buildings is mainly related to their shape and aspect ratio. Tanaka and Tamura<sup>[22]</sup> provided the wind load on 400-m-high tall buildings with 27 different shapes grouped into 7 categories. Moreover, Bandi and Tamura<sup>[23]</sup> evaluated the wind load of tall buildings with various triangular cross-sections including six different shapes. Tanaka and Tamura<sup>[24]</sup> also investigated the flow characteristics around tall buildings with various unconventional configurations. This series of papers represents the most extensive recent research on the wind load on tall buildings, with a comprehensive understanding of the aerodynamic characteristics involved by various shapes. However, when the building height reaches 1,000 m-high, the wind flow around the building may become very different and even more very uncertain especially with reference to the oncoming turbulence and its effects on the wind loading mechanisms.<sup>[25]</sup> This leads to the need of investigating the aerodynamic characteristics of 1,000 m-high super-tall buildings on taking duly into account the modified properties of the oncoming flow.

Many wind codes provide the profile of the mean wind speed and turbulence intensity based on the Power Law,<sup>[26–28]</sup> an empirical model without a sound supporting theory. In this framework, the atmospheric boundary layer (ABL) is only

**TABLE 1** List of buildings with height beyond 500 m

Building name	Height (m)	Country	City	Status
Kingdom Tower	1,000 m	Saudi Arabia	Jeddah	Construction
Burj Khalifa	828 m	United Arab Emirates	Dubai	Completed
Suzhou Zhongnan Center	729 m	China	Suzhou	Construction
Pingan Finance Center	660 m	China	Shenzhen	Construction
Wuhan Greenland Center	636 m	China	Wuhan	Construction
KL 118 Tower	635 m	Malaysia	Kuala Lumpur	Construction
Shanghai Tower	632 m	China	Shanghai	Completed
Makkah Royal Clock Tower Hotel	601 m	Saudi Arabia	Mecca	Completed
Coldin Finance 117	596.5 m	China	Tianjin	Construction
Global Financial Center Tower 1	568 m	China	Shenyang	Construction
Lotte World Tower	554.5 m	Korea	Seoul	Construction
One World Trade Center	541.3 m	Unite states	New York	Completed
Central Part Tower	541 m	Unite states	New York	Construction
Chow Tai Fook Binhai Center	530 m	China	Tianjin	Construction
China Zun Tower	528 m	China	Beijing	Construction
Dalian Greenland Center	518 m	China	Dalian	Construction
Taipei 101	508 m	China	Taipei	Completed

Note. This table is extracted from “100 Future Tallest Building in the world” in the website of the Skyscraper Center, <http://skyscrapercenter.com>.

defined as the atmospheric region affected by the roughness of the ground surface directly, and the height of the ABL is empirically specified as 300–550 m according to the roughness of the terrain. This is the maximum height provided for the wind profile. Other wind codes adopt the profile of the mean wind speed and turbulence intensity based on the Logarithmic Law,<sup>[29]</sup> a model founded on a robust supporting theory. In this framework, the height of the ABL assumes values in the order of 3,000–5,000 m according to the roughness of the terrain, the wind speed, and the site latitude. However, as indicated by most codes, the wind profile is assigned and may be applied up to about 200 m, that is, the height of the inner boundary layer in which the mean wind speed direction and the turbulence standard deviation (SD) are nearly independent of height. These design concepts are acceptable in most cases, but not appropriate when the building height exceeds 500 m.<sup>[30]</sup> Under this viewpoint, more complex models that involve advanced atmospheric physics and boundary layer theory concepts are needed. In addition, at least in principle, the wind deflection caused by Coriolis force has to be considered in the wind load simulations. In any case, these problems need further research.

Typhoon is another important issue for designing 1,000 m-high super-tall buildings close to the seaside. Compared with the monsoon climate wind flow, the typhoon climate wind flow is more complex, a limited number of investigations is available, and many characteristics of this atmospheric phenomenon are still unknown. However, a lot of data based on field measurements have been reported by Vickery et al.<sup>[31,32]</sup> and Tse et al.<sup>[33]</sup> with reference to the mean wind speed profile. These data point out properties that are totally different from those of monsoons, especially the presence of an inflection point in the mean wind speed profile. Because the inflection point is usually below 1,000 m, this surely affects the aerodynamic load on 1,000 m-high buildings. As far as concerns fluctuations, the data collected by Song et al.,<sup>[34]</sup> Cao et al.,<sup>[35]</sup> and Li et al.<sup>[36]</sup> confirm that turbulence intensity in typhoons is usually higher than that in monsoons; however, the power spectrum of turbulence in typhoon wind flows typically matches the Karman-type function commonly adopted in monsoon wind flows except for the eye region. In any case, the typhoon wind load on super-tall buildings needs a separate assessment and further research, especially on the effects of the inflection point on the mean wind speed profile.

This paper illustrates a preliminary study of the aerodynamic wind load on 1,000 m-high super-tall buildings. After this introduction, Section 2 provides an outline of the high-frequency force balance (HFFB) tests carried out in the boundary layer wind tunnel at the Beijing Jiaotong University by simulating both monsoon and typhoon climate wind flows; special attention is put on the choice of the target wind velocity properties and on the devices realized to reproduce these in the case of typhoons. Sections 3 and 4 discuss the crucial role, respectively, of the building height and of the properties of the oncoming flow. Section 5 summarizes the main conclusions and provides some prospects.

## 2 | OUTLINE OF WIND TUNNEL TESTS

### 2.1 | Test model

Five buildings with square plan have been selected for HFFB tests (Figure 1). They have heights 600 m (I); 800 m (II); 1,000 m (III); 1,200 m (IV); and 1,500 m (V) with aspect ratio 8, the same as that studied by Tanaka and Tamura.<sup>[22]</sup> The number in brackets denotes the building serial number.

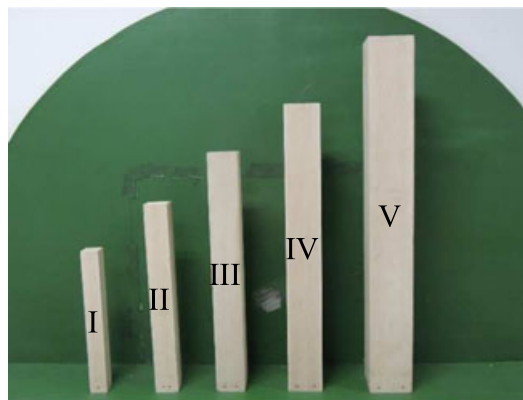


**FIGURE 1** Test models

According to the size of the closed-circuit wind tunnel at Beijing Jiaotong University, the geometric scale of the models is set at 1/1,500. The HFFB models are made by 5-mm-thick Balsa Wood in order to reduce their mass. The high-frequency balance (made by ATI Industrial Automation) was mounted at the base of each model to simulate a rigid base connection at the ground of the turntable in the wind tunnel.

The sampling frequencies of the test system are 138 Hz (I), 106 Hz (II), 93 Hz (III), 66 Hz (IV), and 47 Hz (V). Only model V seems to be a bit flexible for HFFB tests.<sup>[37,38]</sup> Therefore, limited to the model V, only the case of mean wind loads has been investigated in this paper. A summary of the parameters of the test models is listed in Table 2.

## 2.2 | Wind flow

Two wind-flow conditions have been investigated herein, the monsoon (section 2.2.1), and typhoon (section 2.2.2) climate wind flows, based on target models suggested in literatures. The choice of these models is motivated and discussed below even though, in the spirit of preliminary analyses, no sensitivity study has been carried out with regard to the many uncertainties involved in these models and in their applications, especially in the field of extreme values of the height above ground; such analyses will be justified especially in the light of new wind field monitoring campaigns in the outer boundary layer.

### 2.2.1 | Monsoon wind flow

According to atmospheric physics and boundary layer theories, the height  $h$  of the top of the ABL, or gradient height, is in the range of 3,000–5,000 m. The ABL may be further divided into the inner boundary layer (or surface layer) and the outer boundary layer (or Ekman layer). Models reported below are circumscribed to neutrally stratified atmospheric conditions.

The inner boundary layer extends up to 1/10 of the height of the ABL. Here, the logarithm law can be used to describe the mean wind speed profile:

$$\frac{U}{u_*} = \frac{1}{k} \ln\left(\frac{z}{z_0}\right), \quad (1)$$

in which  $U$  is the mean wind speed at height  $z$ ;  $u_*$  is the shear velocity;  $k$  is the Von Karman's constant with a mean numerical value of 0.4; and  $z_0$  is the roughness length of the terrain.

The outer boundary layer covers the remaining 9/10 of the height of the ABL, where the wind speed changes gently along the height. Here, the velocity defect law is usually employed to define the mean wind speed profile:

$$\frac{G-U}{u_*} = \frac{1}{k} \left[ \ln\left(\frac{u_*}{F_c z_0}\right) + A \right], \quad (2)$$

in which  $G$  is the gradient wind speed;  $F_c$  is the Coriolis parameter (around  $10^{-4}$  for temperate latitudes); and  $A$  is a constant ( $A = 1$  is usually suggested).

Deaves and Harris<sup>[39]</sup> (D-H) made a “matching” between the properties of the inner and outer boundary layers in order to form a composite solution of the mean wind speed profile applicable to the whole ABL. Based on asymptotically similarity<sup>[40]</sup> and field measurements carried out in Nantes, Rugby, Grandfield, Leipzig, and Farnborough, they proposed the law<sup>[39]</sup>

**TABLE 2** Summary of the parameters of the test models

Model number	Prototype building		Test model		Blockage ratio	System frequency
	Height	Side	Height	Side		
I	600 m	75 m	400 mm	50 mm	0.33%	138 Hz
II	800 m	100 m	533 mm	67 mm	0.60%	106 Hz
III	1,000 m	125 m	667 mm	83 mm	0.92%	93 Hz
IV	1,200 m	150 m	800 mm	100 mm	1.33%	66 Hz
V	1,500 m	187.5 m	1,000 mm	125 mm	2.08%	47 Hz

$$\frac{U}{u_*} = \frac{1}{k} \left[ \ln\left(\frac{z}{z_0}\right) + 5.75\left(\frac{z}{h}\right) - 1.88\left(\frac{z}{h}\right)^2 - \frac{4}{3}\left(\frac{z}{h}\right)^3 + \frac{1}{4}\left(\frac{z}{h}\right)^4 \right], \quad (3)$$

where the gradient height may be calculated as

$$h = \frac{1}{\beta} \frac{u_*}{F_c}, \quad (4)$$

where  $\beta$  is a constant ( $\beta = 6$  is usually suggested).

Then, the longitudinal turbulence intensity  $I_u$  can be written as

$$I_u = \frac{\sigma_u u_*}{u_* U}, \quad (5)$$

$$\frac{\sigma_u}{u_*} = \frac{7.5\eta[0.538 + 0.09 \ln(z/z_0)]^p}{1 + 0.156 \ln(u_*/(fz_0))}; \quad \eta = 1 - 6fz/u_*; \quad p = \eta^{16}. \quad (6)$$

Models providing the lateral and vertical turbulence intensities are reported for instance by Solari and Piccardo<sup>[41]</sup> and by Solari and Tubino.<sup>[42]</sup>

Deaves and Harris<sup>[43]</sup> also provided the following expression of  $\theta_g$ , namely, the total angle of turn of the mean wind speed throughout the ABL:

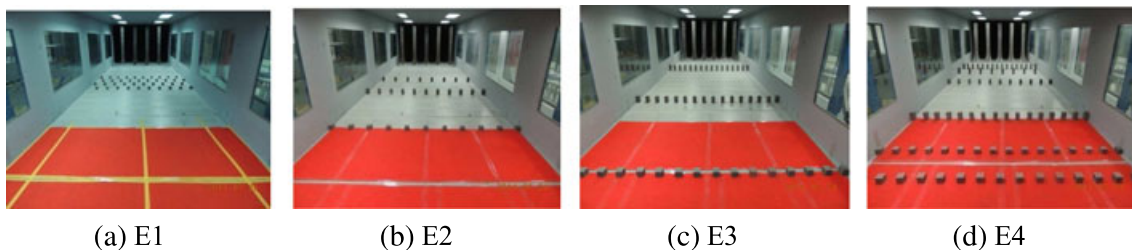
$$\frac{G \sin \theta_g}{u_*} = 2\beta. \quad (7)$$

Table 3 shows the parameters of the ABL taking Beijing as a typical example of a big city located inland in a Monsoon wind climatology. The design wind speed at 10-m high as provided by the Chinese Load Code<sup>[28]</sup> is  $U_{10} = 28.8$  m/s;  $U_{10} = 30$  m/s has been used herein for sake of simplicity. The angle of turn of the mean wind speed at 1,000-m height,  $\theta_{1,000}$ , has been predicted for three different values of the roughness using the assumption of uniform velocity rotation. Because the value of  $\theta_{1,000}$  is quite small, its effects are ignored.

The D-H model described above, recommended by ESDU 82026<sup>[44]</sup> and ISO 4354,<sup>[45]</sup> is adopted here as a target to simulate the wind flow in wind tunnel tests, as it is classical, using an appropriate mix of spires installed at the entrance of the test section and floor roughness elements. Four kinds of terrain have been considered in this study with roughness lengths  $z_0 = 0.036$  m (E1), 0.096 m (E2), 0.288 m (E3), and 0.653 m (E4; Figure 2). They represent Open Terrain, Countryside Terrain, Suburban Terrain, and Urban Terrain ( $z_0$  is about 0.03, 0.1, 0.3, and 0.7 m) conditions, respectively.

**TABLE 3** Parameters of the ABL

$U_{10}$ (m/s)	$z_0$ (m)	$u_*$ (m/s)	$\theta_g$ (°)	$\theta_{1,000}$ (°)
30	0.03	2.07	19.4	5.6
30	0.3	3.42	22.3	3.9
30	0.7	4.51	23.4	3.1



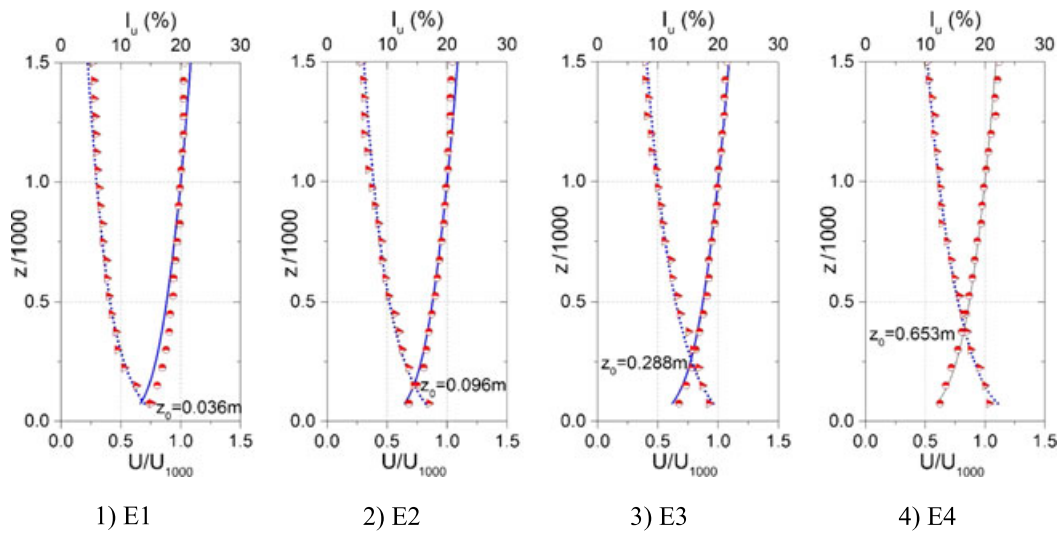
**FIGURE 2** Monsoon wind-flow simulation in the wind tunnel

Figure 3 shows a comparison between the target and simulated profiles of the mean wind speed and longitudinal turbulence intensity. A wind flow similar to E3 ( $z_0 = 0.288$  m) is usually considered for super-tall building design, such as in the case of the China Zun Tower (528 m) in Beijing.<sup>[46]</sup>

Table 4 gives detailed information on the longitudinal, lateral, and vertical turbulence intensities and integral length scales for wind flow E3.

Turbulence intensities decrease on increasing the height above ground and  $I_u > I_v > I_w$  as expected. However, the ratios  $I_u : I_v : I_w$  do not perfectly match the common values drawn from field measurements in monsoon climate wind flow, namely, (1.9–2.0):1.5:1.0 for instance according to Solari and Piccardo<sup>[41]</sup> and Teunissen.<sup>[47]</sup> In particular, the lateral turbulence component measured in wind tunnel is small.

Turbulence integral length scales  $L_{ux}$ ,  $L_{vx}$ ,  $L_{wx}$  have been estimated by the zero value of the power spectral density (PSD) of turbulence as suggested by Cao and Tamura.<sup>[35]</sup> Their reliability has been checked by comparing the experimental PSD with that obtained by substituting the measured turbulence integral length scales in the Karman-type PSD as provided by Katsuchi and Yamada.<sup>[48]</sup> Examples (550-mm height in wind tunnel; 825-m height in full scale) of this comparison are shown in Figure 4, where  $f$  is the frequency; the agreement is very good. However, turbulence integral length scales do not increase on increasing the height above ground, and  $L_{vx} < L_{wx}$  is contrary to common values drawn from



Note: Blue solid and dotted lines refer to the target mean wind speed and longitudinal turbulence intensity profiles, respectively; half-red circle and triangle dots refer to the mean wind speed and longitudinal turbulence intensity profiles, respectively, as simulated in wind tunnels.

**FIGURE 3** Wind profiles in wind tunnel (monsoon)

**TABLE 4** Turbulence parameters of monsoon climate wind flow E3

Height in wind tunnel	Turbulence intensity			Turbulence integral length scale		
	$I_u$	$I_v$	$I_w$	$L_{ux}$ (m)	$L_{vx}$ (m)	$L_{wx}$ (m)
50 mm	18.5%	8.33%	10.2%	0.27	0.05	0.23
150 mm	16.8%	8.67%	8.65%	0.43	0.08	0.25
250 mm	15.1%	8.15%	7.48%	0.48	0.13	0.23
350 mm	13.3%	7.36%	6.52%	0.49	0.13	0.23
450 mm	12.2%	7.10%	6.19%	0.42	0.14	0.22
550 mm	10.8%	6.65%	5.62%	0.43	0.14	0.22
650 mm	10.0%	6.05%	5.25%	0.34	0.15	0.20
750 mm	8.97%	5.81%	4.80%	0.34	0.14	0.21
850 mm	8.23%	5.66%	4.38%	0.27	0.16	0.19

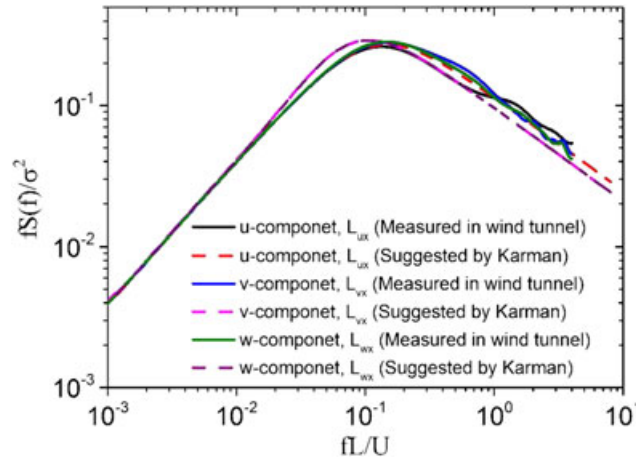


**FIGURE 4** Power spectral densities of wind flow E3 in the wind tunnel

field measurements.<sup>[41]</sup> These results may be explained considering that, due to the wall constraint effects caused by the side walls, the ceiling and the floor, flow in wind tunnel cannot be the same as an ideal neutral situation or full-scale conditions near the ground.

### 2.2.2 | Typhoon wind flow

China is a huge country, and there are many famous big cities located close to the seaside, such as Shanghai, Shenzhen, and Hong Kong. The design wind speed in these areas is close to 40 m/s at 10-m height, this depending on Typhoons not on Monsoons. According to field measurement results, the mean wind speed profile of typhoons exhibits an inflection point whose height is usually lower than 1,000 m.<sup>[27,28]</sup> This is worth noting because it implies that the mean wind speed no longer increases with height from the terrain to 1,000 m. The D-H wind profile is therefore not suitable in this case.

According to the model suggested by Vickery and Powell<sup>[32]</sup> (V-P) for engineering applications related to hurricanes based on 896 recorded vertical profiles, the mean wind speed profile of Typhoons is schematized as

$$U(z) = \frac{u_*}{k} \left[ \ln\left(\frac{z}{z_0}\right) - a\left(\frac{z}{H^*}\right)^n \right], \quad (8)$$

in which  $H^*$  is referred to as the boundary layer height parameter;  $a$  and  $n$  are constant parameters for which Vickery and Powell<sup>[32]</sup> suggested to adopt  $a = 0.4$  and  $n = 2.0$ . Using these values and setting the derivative of  $U$  with respect to  $z$  as equal to zero, that is,  $\partial U(z)/\partial z = 0$ , the height of the inflection point, that is, the height at which  $U$  is maximum, is given by

$$H_F = 1.12H^*. \quad (9)$$

According to Kepert,<sup>[49]</sup>  $H^*$  is inversely proportional to  $\sqrt{I}$ ,  $I$  being the inertial stability. In addition, Kepert provided the following simple regression model that links  $H^*$  and  $\sqrt{I}$  near and outside the storm radius to maximum winds, namely, the distance between the center of a cyclone and its band of strongest winds:

$$H^* = 186.6 + 12.66/\sqrt{I}, \quad (10)$$

$$I = \sqrt{\left(F_c + \frac{2U_F}{r}\right)\left(F_c + \frac{U_F}{r} + \frac{\partial U_F}{\partial r}\right)} \approx \sqrt{\left(F_c + \frac{2U_F}{r}\right)\left(F_c + \frac{U_F}{r}\right)}, \quad (11)$$

in which  $r$  is the radial distance from the center of the storm;  $U_F$  is the mean wind speed at the inflection point. In this paper,  $U_{10} = 40\text{m/s}$ ,  $z_0 = 0.002\text{m}$ ,  $r = 50\text{km}$ , and  $H^* = 500\text{m}$  are used.

As far as concerns the longitudinal turbulence intensity, based on field measured data reported by Song et al.,<sup>[34]</sup> Cao et al.,<sup>[35]</sup> and Li et al.,<sup>[36]</sup> it has been estimated as  $I_u = 10\text{--}15\%$ . This band of values is usually a little larger than that experienced in strong monsoon winds.

Figure 5 shows the setup of the wind tunnel by means of which the above target typhoon wind flow has been simulated. In particular, five concave spires connected by seven lateral grilles at the upper half part of the model have been used. At authors' knowledge, this is the first time that such devices are used to simulate a typhoon climate wind flow, or a wind-flow profile with an inflection point.

Figure 6 shows a comparison between the target and simulated (wind tunnel) profiles of the mean wind speed; in addition, it shows the longitudinal turbulence intensity as measured in wind tunnel tests. According to the measured data, the inflection points of the mean wind speed profiles occur at 576 and 644 m, respectively, for the wind flows T1 and T2. The changing of the longitudinal turbulence intensity along the height is converse with that of the mean wind speed, which means the SD value of the wind speed fluctuation  $\sigma_u$  is independent of height.

Table 5 gives detailed information on the longitudinal, lateral, and vertical turbulence intensities and integral length scales for wind flow T1.

The turbulence intensity and integral length scale exhibit small variations along height above floor. Like the results drawn from the simulated monsoon climate wind flow E3, the intensity and the integral length scale of the lateral turbulence component (v-component) are moderately small.



FIGURE 5 Typhoon wind-flow simulation in the wind tunnel

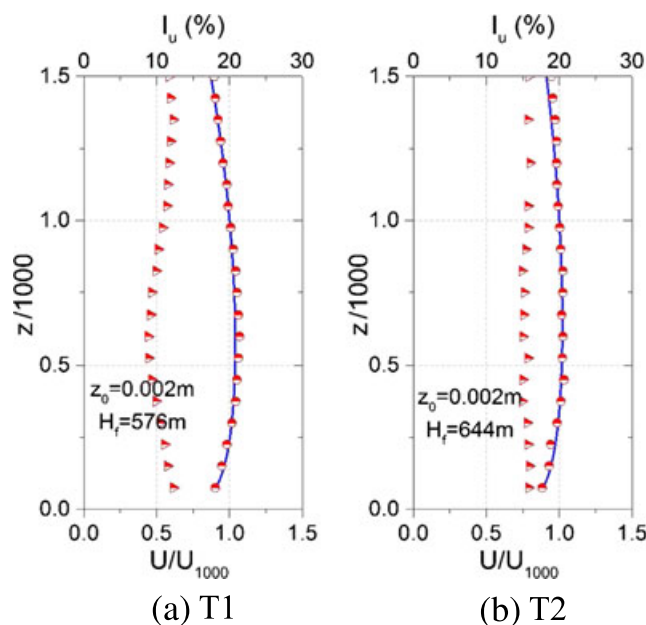


FIGURE 6 Wind profile in wind tunnel (typhoon)



**TABLE 5** Turbulence parameters of typhoon climate wind flow T1

Height in wind tunnel	Turbulence intensity			Turbulence integral length scale		
	$I_u$	$I_v$	$I_w$	$L_{ux}$	$L_{vx}$	$L_{wx}$
50 mm	12.3%	5.61%	6.10%	0.29	0.06	0.18
150 mm	11.1%	6.07%	5.59%	0.28	0.08	0.19
250 mm	9.90%	5.96%	4.96%	0.27	0.10	0.19
350 mm	8.94%	5.83%	4.84%	0.26	0.11	0.21
450 mm	9.16%	6.06%	4.81%	0.26	0.12	0.20
550 mm	9.93%	6.63%	4.98%	0.32	0.15	0.20
650 mm	10.8%	7.03%	5.39%	0.38	0.16	0.18
750 mm	11.5%	7.71%	5.72%	0.36	0.17	0.17
850 mm	11.9%	8.35%	6.19%	0.38	0.18	0.21

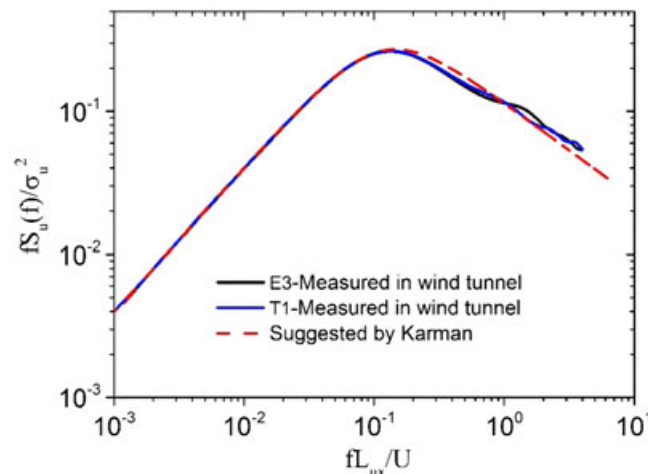
### 2.2.3 | Comparisons and further remarks on monsoon and typhoon wind flows

A summary of the test wind-flow parameters is given in Table 6. As an example, Figure 7 compares the longitudinal PSDs (u-component) of the simulated monsoon climate wind flow E3 and typhoon climate wind flow T1 at the height of 550 mm (825 m in full scale) with the model suggested by Karman. The different diagrams are almost overlapped. Furthermore, the reduced spectral form  $fS_u/\sigma_u^2$  of the two types of wind flow are almost the same at different heights.

Table 7 summarizes the turbulence integral length scales  $L_{ux}$  for all the wind flows simulated in the wind tunnel. As an example, Figure 8 provides the turbulence scale profiles of the simulated wind flows E1, E2, E3, E4 and T1, T2. It is apparent that in all cases, the variation of  $L_{ux}$  along the height is small, and there is no clear trend of the increase of  $L_{ux}$  with the height, which agrees with the results shown by Tieleman.<sup>[50]</sup> The turbulence scale  $L_{ux}$  is larger than the side of

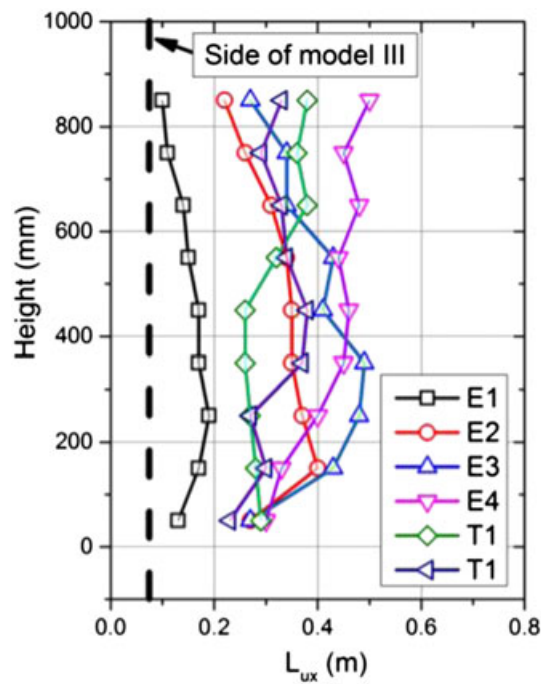
**TABLE 6** Summary of test wind-flow parameters

Climate type	Wind flow number	Terrain	$z_0$ (m)	Inflection point height (m)
Monsoon	E1	Open	0.036	\
	E2	Countryside	0.096	\
	E3	Suburban	0.288	\
	E4	Urban	0.635	\
Typhoon	T1	Seaside	0.002	576
	T2	Seaside	0.002	644

**FIGURE 7** The power spectral densities of the wind flow E3 and T1

**TABLE 7** List of turbulence scale in u-component ( $L_{ux}$ )

Height in wind tunnel	Monsoon climate (m)				Typhoon climate (m)	
	E1	E2	E3	E4	T1	T2
50 mm	0.13	0.27	0.27	0.30	0.29	0.23
150 mm	0.17	0.40	0.43	0.33	0.28	0.30
250 mm	0.19	0.37	0.48	0.40	0.27	0.27
350 mm	0.17	0.35	0.49	0.45	0.26	0.37
450 mm	0.17	0.35	0.41	0.46	0.26	0.38
550 mm	0.15	0.34	0.43	0.44	0.32	0.34
650 mm	0.14	0.31	0.34	0.48	0.38	0.33
750 mm	0.11	0.26	0.34	0.45	0.36	0.29
850 mm	0.10	0.22	0.27	0.50	0.38	0.33
Mean value	0.146	0.317	0.386	0.425	0.311	0.315

**FIGURE 8** Profile of the turbulence scales  $L_{ux}$ 

test models, thus the fluctuating wind load is primarily related to the small-scale turbulence (high frequency part of the PSDs) in the incident flow. As for this issue, Irwin<sup>[51]</sup> even used the “partial simulation approach” to carry out tests in wind tunnel aiming to realize real flow conditions limited to the high-frequency part of the PSD of turbulence.

Katsuchi and Yamada<sup>[48]</sup> introduced another similarity parameter, “the reduced turbulence intensity,” to develop the partial simulation approach based on the Karman-type PSD function. Accordingly, the reduced turbulence intensity  $I_r$  is defined by

$$I_r = \frac{I_u}{(L_{ux}/b)^{1/3}}. \quad (12)$$

Table 8 provides the longitudinal turbulence intensity, the longitudinal turbulence scale, and the reduced turbulence intensity taking Model III (1,000 m-high) as an example. The results show that the reduced turbulence intensity is about 2/3 of the simulated turbulence intensity. Following the ideas of the partial simulation approach and the reduced

**TABLE 8** Further information of E3 and T1 wind flow

Height in wind tunnel	E3 wind flow			T1 wind flow		
	$I_u$ (%)	$L_{ux}$ (m)	$I_r$ (%)	$I_u$ (%)	$L_{ux}$ (m)	$I_r$ (%)
50 mm	18.5	0.27	12.50	12.3	0.29	8.16
150 mm	16.8	0.43	9.72	11.1	0.28	7.41
250 mm	15.1	0.48	8.42	9.9	0.27	6.73
350 mm	13.3	0.49	7.39	8.94	0.26	6.11
450 mm	12.2	0.41	7.13	9.16	0.26	6.25
550 mm	10.8	0.43	6.25	9.93	0.32	6.34
650 mm	10.0	0.34	6.26	10.8	0.38	6.51
750 mm	8.97	0.34	5.64	11.5	0.36	7.07
850 mm	8.23	0.27	5.56	11.9	0.38	7.21

turbulence intensity, the simulated turbulence intensity in wind tunnel is larger than that of prototypes in full scale, as the simulated turbulence scale cannot satisfy the geometrical scale of test models. In addition, it is mentioned that, except E1 wind flow, the geometric scale satisfies the requirement of  $L_{ux}/b > 3$  in ASCE/SEI 49–12.<sup>[52]</sup>

### 2.3 | Base overturning moments

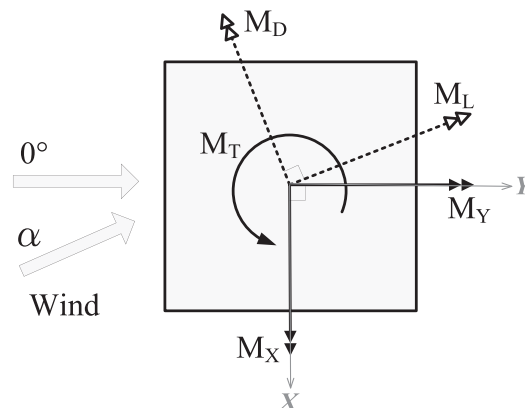
Table 9 summarizes the experimental cases analyzed herein. The overturning moments at the base of the models,  $M_X(t)$  and  $M_Y(t)$ , are recorded with sampling frequency 1,000 Hz. Sixteen 40-s long samples are collected for each case, which correspond to sixteen 10-min long samples in full scale. In every case, the oncoming wind directional angle  $\alpha$  is varied with intervals  $5^\circ$  from  $0^\circ$  to  $45^\circ$ . The coordinate system is shown in Figure 9.

The time histories of the along-wind and across-wind overturning moments,  $M_D(t)$  and  $M_L(t)$ , can be calculated by:

$$\begin{pmatrix} M_L(t) \\ M_D(t) \end{pmatrix} = \begin{pmatrix} \cos(\alpha + 90^\circ) & \sin(\alpha + 90^\circ) \\ -\sin(\alpha + 90^\circ) & \cos(\alpha + 90^\circ) \end{pmatrix} \begin{pmatrix} M_X(t) \\ M_Y(t) \end{pmatrix} \quad (13)$$

**TABLE 9** Experimental cases

	Test model	Wind flow
Group 1	I, II, III, IV, V	E3, T1
Group 2	III	E1, E2, E3, E4, T1, T2

**FIGURE 9** Coordinate system

The along-wind and across-wind overturning moment coefficients,  $C_{MD}(t)$  and  $C_{ML}(t)$ , are defined with reference to the mean wind speed at the top of buildings  $U_h$  as

$$C_{MD}(t) = \frac{M_D(t)}{0.5\rho U_h^2 b h^2}, \quad (14)$$

$$C_{ML}(t) = \frac{M_L(t)}{0.5\rho U_h^2 b h^2}, \quad (15)$$

where  $\rho$  is the density of air, and  $b$  and  $h$  are the width and height of the building, respectively. The mean value of the overturning moment coefficients describes the mean wind load. The SD and the PSD of the overturning moment coefficients define the fluctuating wind load. In this paper, no evaluation is reported for the base shear forces and torque.

### 3 | EFFECT OF BUILDING HEIGHT ON WIND LOAD

The influence of building height on wind load has been investigated taking test results for the E3 wind flow as an example of the Monsoon climate (section 3.1) and those for the T1 wind flow as an example of the Typhoon climate (section 3.2). Although results for monsoon climate can be regarded as rather classic, they represent a useful reference point to comment the variations that occur in the less classic case of typhoon climate.

#### 3.1 | Monsoon climate

##### 3.1.1 | Along-wind overturning moment coefficients

The overturning moment coefficients in the along-wind direction are given in Figure 10 for the wind flow E3 as a function of the wind direction  $\alpha$ . Their trend agrees with that provided by Tanaka and Tamura.<sup>[22]</sup> On increasing the height of the building, the mean coefficients (Figure 10a) remain almost the same whereas their SD (Figure 10b) decrease due to the reduction of turbulent fluctuations. In addition, the variation of both these coefficients with the wind direction is almost the same for buildings with different height.

The PSD of the overturning moment coefficients in the along-wind direction of Model III is shown as an example in Figure 11 as a function of the reduced frequency  $fB/U_H$ . On varying the wind direction, they remain almost constant, which means that there is no change in the wind load mechanism.

The PSDs at  $\alpha = 0^\circ$  for different heights of the model are shown in Figure 12. As their shapes is almost the same on varying the height, the along-wind load mechanism remains unchanged. However, the PSDs exhibit translation toward the right on increasing the height, as the parameter  $b/L_{ux}$  takes the values 0.13, 0.17, 0.22, and 0.26 for Models I, II, III,

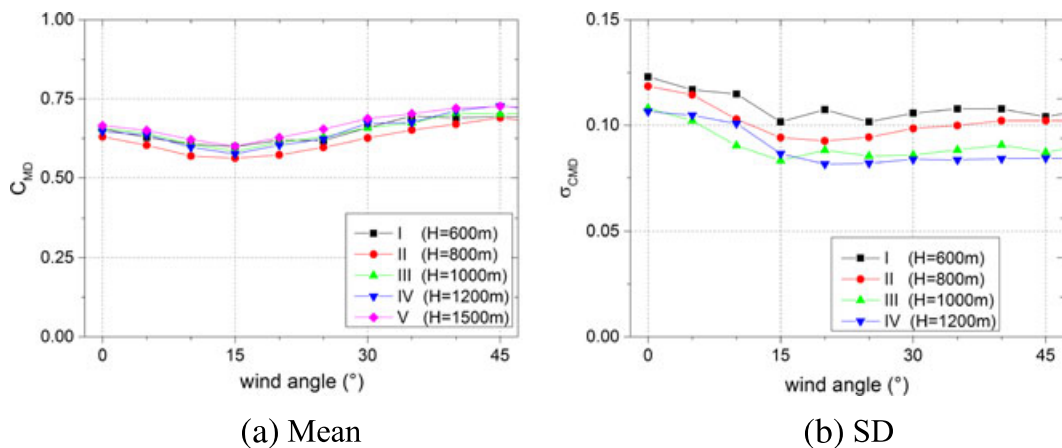


**FIGURE 10** Along-wind overturning moment coefficients (wind flow E3). SD = standard deviation

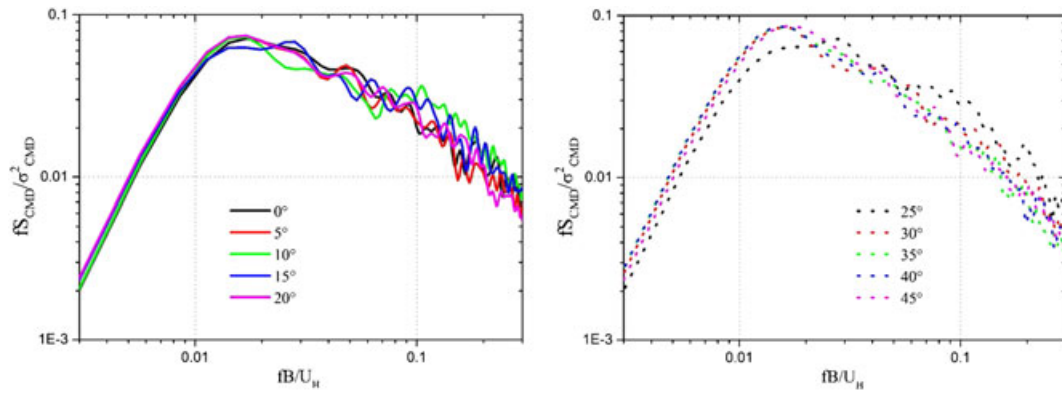


**FIGURE 11** Power spectral density of the overturning moment coefficients in along-wind direction (Model III, E3)

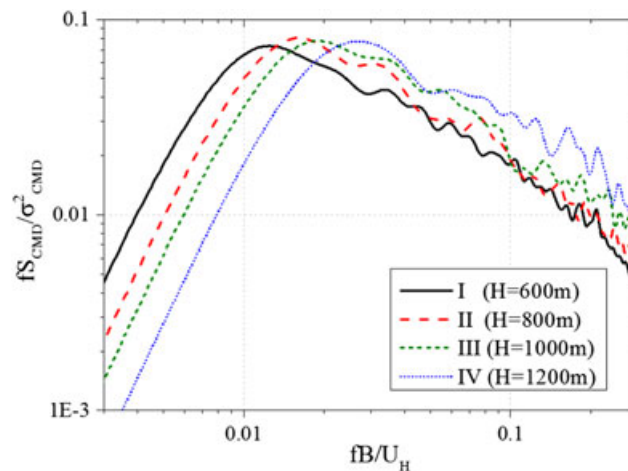


**FIGURE 12** Power spectral density of the overturning moment coefficients in the along-wind direction (E3,  $\alpha = 0^\circ$ )

and IV, respectively. On the other hand, larger  $b/L_{ux}$  usually causes distortion (or more energy dissipation) in the high frequency range, this resulting in a fast decrease of the PSD curve; however, this phenomenon is not obvious in the figure.

Comparing Figure 12 with Figure 4, it may be observed that the along-wind load and overturning moment primarily result from pressure fluctuations on the windward face and generally follow the fluctuations in the approaching flow. The wind direction has little influence on the PSD of the along-wind overturning moment coefficient. However, the turbulent intensity decreases with increasing the height of the building, and these results in smaller fluctuating overturning moment coefficients in the along-wind direction.

Also, pressure fluctuations on the leeward face contribute to the along-wind load and overturning moment through a weak shedding downstream mechanism; the dominant reduced frequency is about 0.2, which is, as expected, nearly twice the Strouhal number. When the turbulence intensity of the wind is low, the weak shedding becomes more apparent. Therefore, when the height of the building is close or exceeds 1,000 m-high, the high-frequency energy of the along-wind fluctuating load slightly increases. The consequences of this effect on the wind-induced response deserve to be studied especially with reference to the wind-induced acceleration.

### 3.1.2 | Across-wind overturning moment coefficients

Figure 13 shows the across-wind overturning moment coefficients. Also, in this case, their trend agrees with that provided by Tanaka and Tamura.<sup>[22]</sup> On increasing the height of the building, the mean coefficients (Figure 13a) increase whereas their SDs (Figure 13b) remain almost unchanged. The mean coefficients exhibit the maximum value for  $\alpha$  in the range  $10^\circ$  to  $15^\circ$ ; the SDs decrease on increasing  $\alpha$ . The variation of both these coefficients with the wind direction is almost the same for buildings with different height.

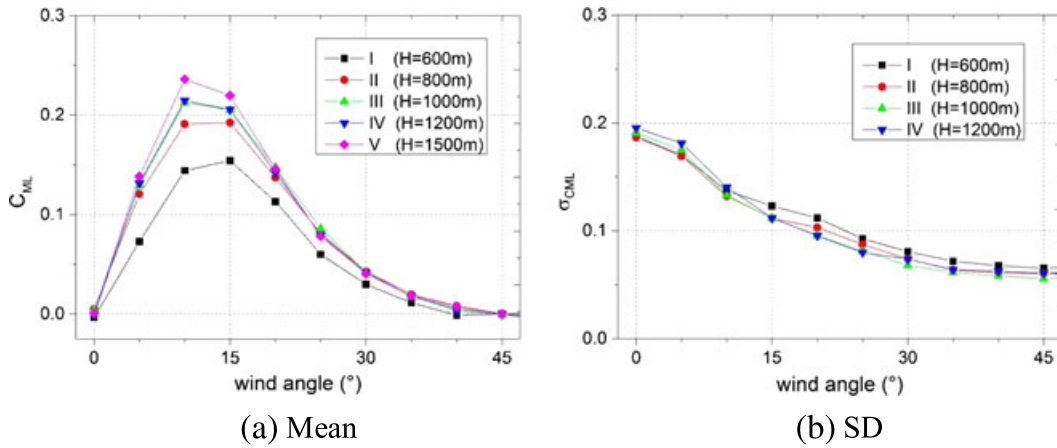


FIGURE 13 Overturning moment coefficients in the across-wind direction (wind flow E3). SD = standard deviation

The PSD of the overturning moment coefficients in the across-wind direction of Model III is shown as an example in Figure 14 as a function of the reduced frequency. There is an obvious peak when the reduced frequency is about 0.1 in all cases, which is mainly caused by the vortex excitation on the sideward faces. The peak value of the PSD is almost the same until the wind direction reaches 15°. When the wind direction changes from 15° to 25°, the peak value decreases sharply. Then, over 25°, the peak value increases slowly with increasing the wind direction.

Figure 15 shows the PSD of the overturning moment coefficients in the across-wind direction for different models; the wind direction is  $\alpha = 0^\circ$ . The turbulence intensity decreases on increasing the height of the building, and this gives

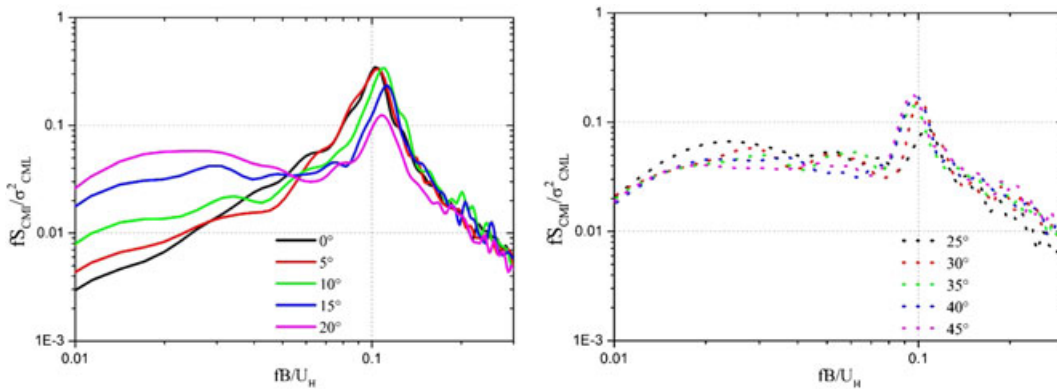


FIGURE 14 Power spectral density of the overturning moment coefficients in the across-wind direction (Model III, E3)

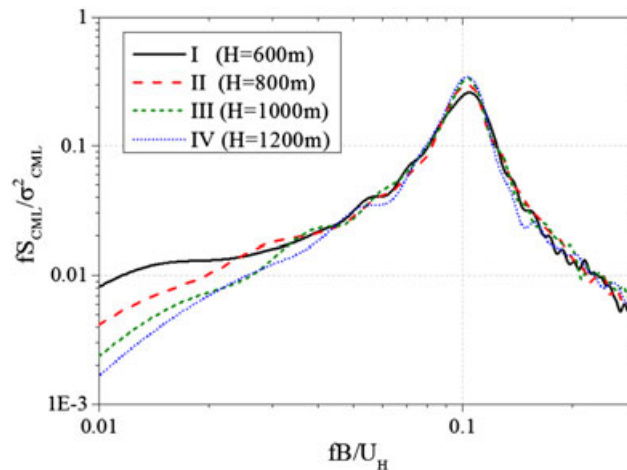


FIGURE 15 Power spectral density of the overturning moment coefficients in the across-wind direction (E3,  $\alpha = 0^\circ$ )

rise to stronger vortex excitations. In fact, the value of the fluctuating across-wind overturning moment coefficients remains almost the same whereas the harmonic content of the vortex excitation tends to become narrower around the peak at the reduced frequency 0.1.

Summarizing, the mean along-wind overturning moment coefficients and the fluctuating across-wind overturning moment coefficients remain almost the same when the building height increases. Because the turbulence intensity in the range of 1,000 m-high buildings is smaller when compared with that for lower buildings, on increasing the building height, the fluctuating along-wind overturning moment coefficients reduce, and more energy is concentrated at the dominant reduced frequency of the fluctuating across-wind load. This will cause stronger structural across-wind vibrations. Because the across-wind response of buildings is a crucial item for their wind-resisting design, attention must be paid and studies are needed to clarify the effects of the stronger vortex actions on increasing the building height.

## 3.2 | Typhoon climate

### 3.2.1 | Along-wind overturning moment coefficients

The along-wind overturning moment coefficients measured in the T1 test flow are given in Figure 16 as a function of the wind direction  $\alpha$ .

The effects of the building height are larger compared with the results from the E3 test flow (Figure 10). Both the mean (Figure 16a) and the SD (Figure 16a) of these coefficients increase on increasing the building height. It is worth noting, however, that also in this case, the overturning moment coefficients are evaluated with reference to the mean wind speed at the top of building  $U_H$ , whereas the calculated inflection point of the mean wind speed profile occurs at 576-m height, that is, all the models are higher than the inflection point and  $U_H$  decreases on increasing the building height. So the results are probably caused by the decrease of  $U_H$ .

Similar to the discussion on the monsoon climate (Figure 11), the PSDs of the along-wind overturning moment coefficients of Model III as a function of the reduced frequency remain the same on changing the wind direction (Figure 17). The PSDs at  $0^\circ$  are given in Figure 18. It is clear that the shape of the PSDs is different from that measured for the wind flow E3 (Figure 12). After reaching the peak value, the PSDs exhibit a plateau, then they decrease slowly at higher frequencies, which means that distortion is smaller in typhoon climate wind flow compared with monsoon climate wind flow. Parameter  $b/L_{ux}$  is 0.16, 0.21, 0.27, and 0.32 for Models I, II, III, and IV, respectively, in wind flow T1. So translation toward right occurs in the PSD of the along-wind overturning moment coefficient with increasing of the height, like in wind flow E3. However, the slopes of the PSDs curves in the high-frequency dissipation range become larger, which means that distortion becomes clearer when parameter  $b/L_{ux}$  rises. Furthermore, the PSD peaks around the reduced frequency 0.2 in Figure 18 are caused by the weak vortex downstream. These peaks are not so clear in Figure 12 related to the monsoon climate due to the larger turbulence intensity in the wind flow E3 as compared with that in the wind flow T1 (Table 5).

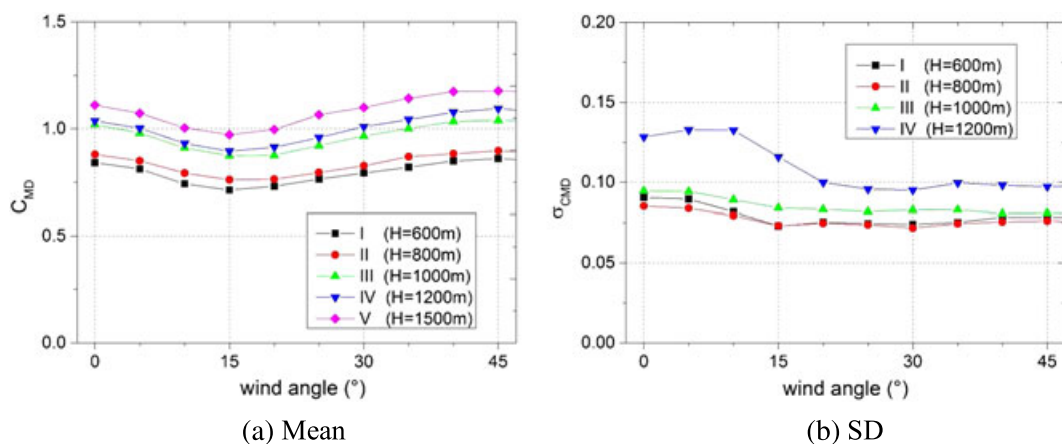


**FIGURE 16** Along-wind overturning moment coefficients (wind flow T1). SD = standard deviation

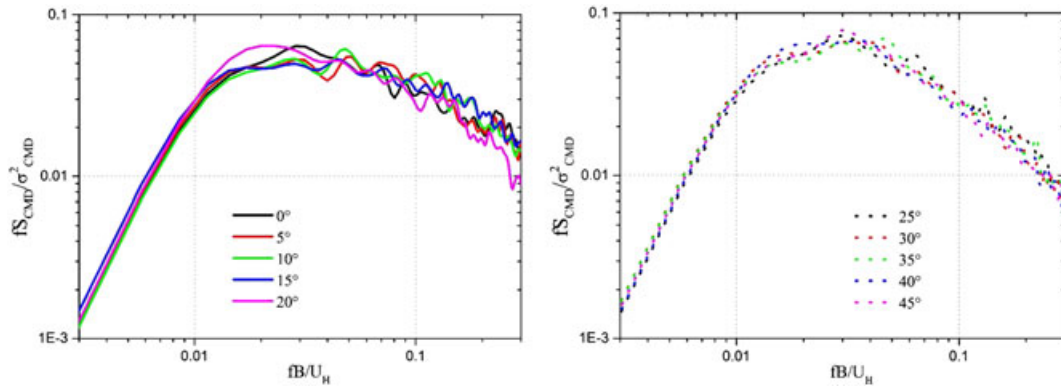


FIGURE 17 Power spectral density of the overturning moment coefficients in the along-wind direction (Model III, T1)

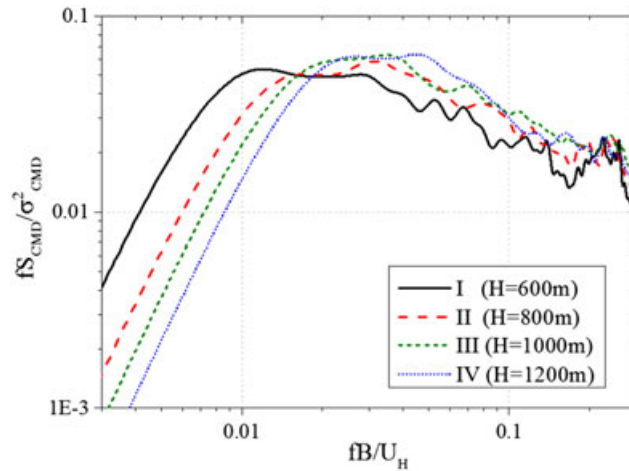


FIGURE 18 Power spectral density of the overturning moment coefficients in the along-wind direction (T1,  $\alpha = 0^\circ$ )

### 3.2.2 | Cross-wind overturning moment coefficients

As shown in Figure 19, likewise in Figures 13 and 16, the building height is an important factor for the across-wind overturning moment coefficient. As mentioned earlier, this is mainly caused by the decreasing of the mean wind speed  $U_H$ . The across-wind load, however, is closely related to the turbulence intensity of the approaching flow and the building shape.

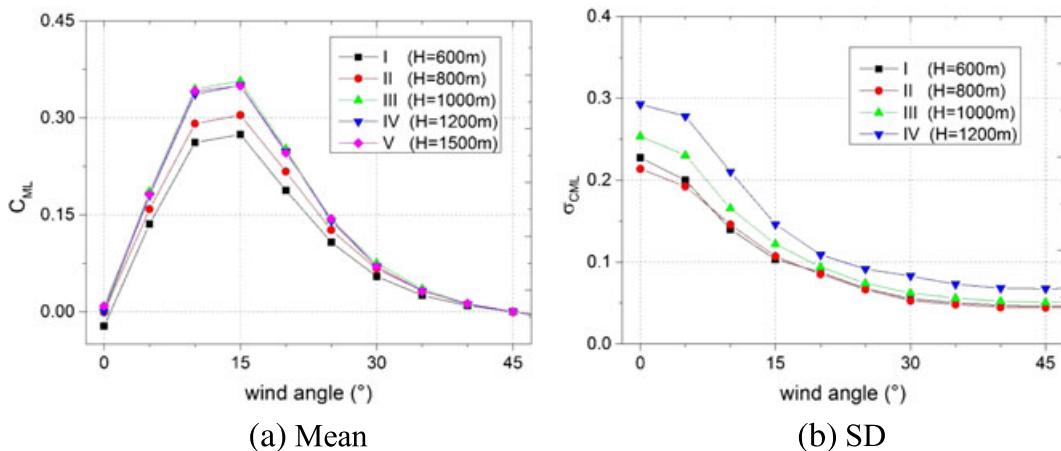


FIGURE 19 Overturning moment coefficients in the across-wind direction (wind flow T1). SD = standard deviation



The PSDs of the across-wind overturning moment coefficients of Model III are provided in Figure 20 as a function of the reduced frequency. Compared with the results related to the monsoon climate (Figure 14), in the typhoon climate, the peak value of the PSD decreases more quickly on increasing the wind direction. The peak induced by vortex excitation on sideward faces is no longer obvious when the wind angle reaches  $20^\circ$ . In addition, the Strouhal number is not 0.1 but increases from 0.12 to 0.14 when the wind angle changes from  $0^\circ$  to  $20^\circ$ .

Figure 21 shows the PSD of the across-wind overturning moment coefficients of different models for  $\alpha = 0^\circ$ . It is worth noting that, reversing the behavior observed in the monsoon climate (Figure 15), the vortex excitation becomes weaker on increasing the building height. In addition, using the mean wind speed at the top of buildings  $U_H$ , as it is common, the Strouhal number increases on increasing the building height.

Summarizing, the overturning moment coefficients become larger when the building height increases, mainly as a consequence of the decreasing of  $U_H$  in the typhoon climate wind flow. Furthermore, the vortex excitation in the across-wind direction becomes weaker on increasing the building height, this behavior being different from that observed in the monsoon climate. It is also mentioned that distortions of wind load in along-wind direction are smaller in typhoon climate wind flows.

### 3.3 | Characteristic turbulence intensity

In order to better explain the above behaviors, a new parameter referred to as the characteristic turbulence intensity  $I_{char}$  is defined herein as the mean value of the turbulence intensities weighted by the product of the heights  $z_i$  at which they are measured in the range of the building and the corresponding tributary height  $\Delta z_i$ :

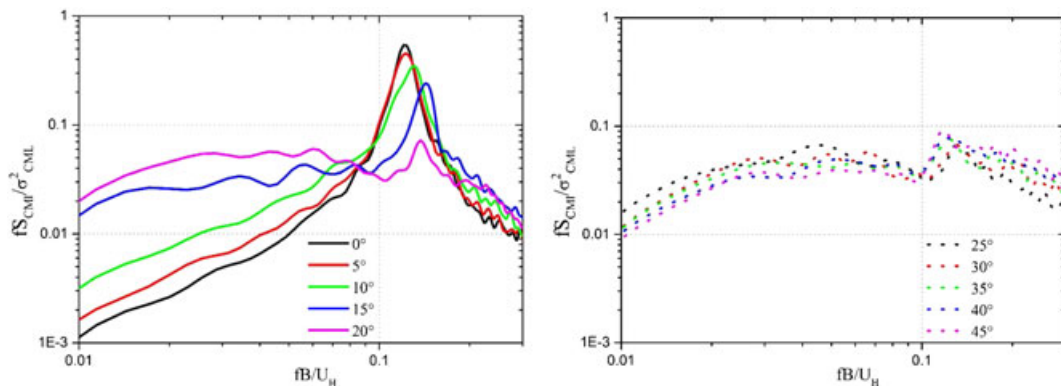


FIGURE 20 Power spectral density of the overturning moment coefficients in the across-wind direction (Model III, T1)

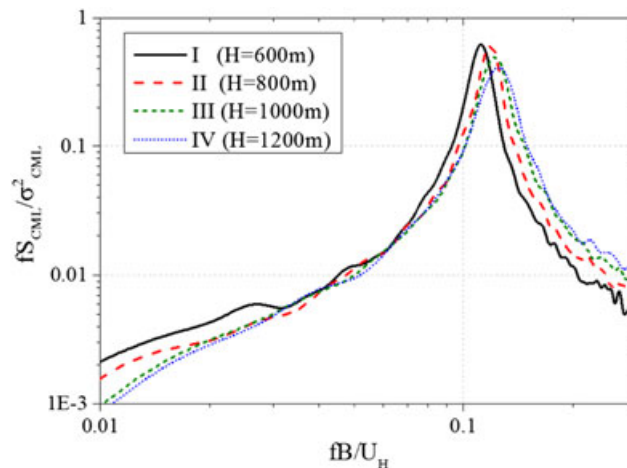


FIGURE 21 Power spectral density of the overturning moment coefficients in the across-wind direction (T1,  $\alpha = 0^\circ$ )

$$I_{char} = \frac{\sum_{i=1}^n I_u(z_i) \cdot \Delta z_i \cdot z_i}{\sum_{i=1}^n \Delta z_i \cdot z_i}, \tag{16}$$

in which  $I_u(z_i)$  is the turbulence intensity at the  $i$ th measurement point ( $i = 1, \dots, n$ ).

It is worth noting that, on increasing the building height, the parameter  $I_{char}$  decreases in the wind flow E3 but increases in the wind flow T1 except for Model I whose height is close to the inflection point of the mean wind speed profile (Table 10). Therefore, the characteristic turbulence intensity  $I_{char}$  can be used to interpret the vortex excitation on super-tall buildings located in different wind flow and climate conditions. The role of this new parameter will be apparent in section 4.3.

### 4 | EFFECTS OF WIND FLOW ON WIND LOAD

The effects of wind flow on wind load are discussed in this section taking Model III with 1,000-m height as an example. Analyses reported below are carried out with the same motivations and in the same spirit related to Section 3.

TABLE 10 Characteristic turbulence intensity

Flow	Model I (600 m high)	Model II (800 m high)	Model III (1,000 m high)	Model IV (1,200 m high)	Model V (1,500 m high)
E3	14.42%	13.46%	12.26%	11.24%	10.25%
T1	9.76%	9.58%	9.88%	10.43%	10.92%

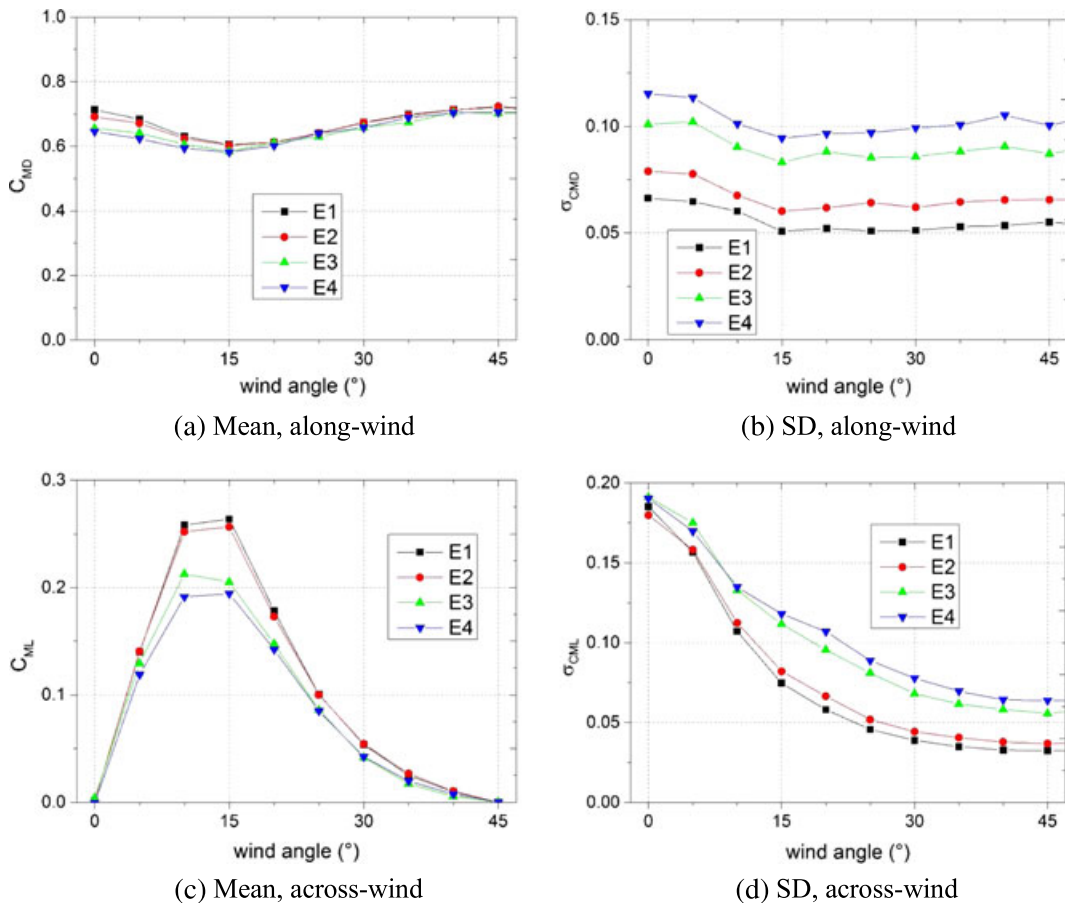
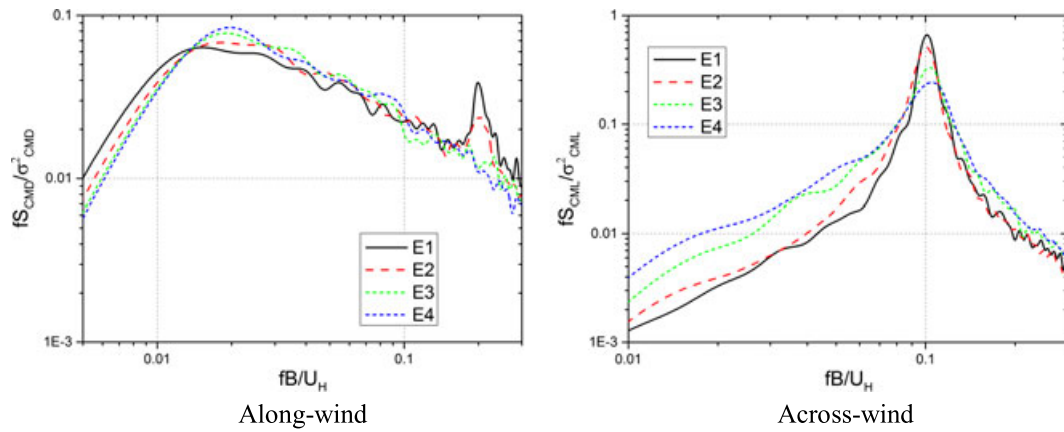


FIGURE 22 Overturning moment coefficients (Model III, monsoon). SD = standard deviation

### 4.1 | Monsoon climate

The overturning moment coefficients of Model III in wind flows E1, E2, E3, and E4 are shown in Figure 22. The corresponding PSDs are shown in Figure 23.

It is worth noting that the overturning moment coefficient clearly depends on the wind flow. On increasing the terrain roughness, the mean coefficients decrease and the value of the fluctuating coefficients increase, both in the along-wind and across-wind directions. The PSDs of the fluctuating wind load (Figure 23) are related to the turbulence intensity. When the turbulence intensity is low or the terrain is smooth, the vortex shedding is stronger. On the one hand, these results in more energy concentrated around the dominant reduced frequency 0.1 of the across-wind load. On the other hand, this causes distinct peaks in the PSDs of the along-wind load at the reduced frequency 0.2, that is,



**FIGURE 23** Power spectral density of the overturning moment coefficients (Model III,  $\alpha = 0^\circ$ , monsoon)

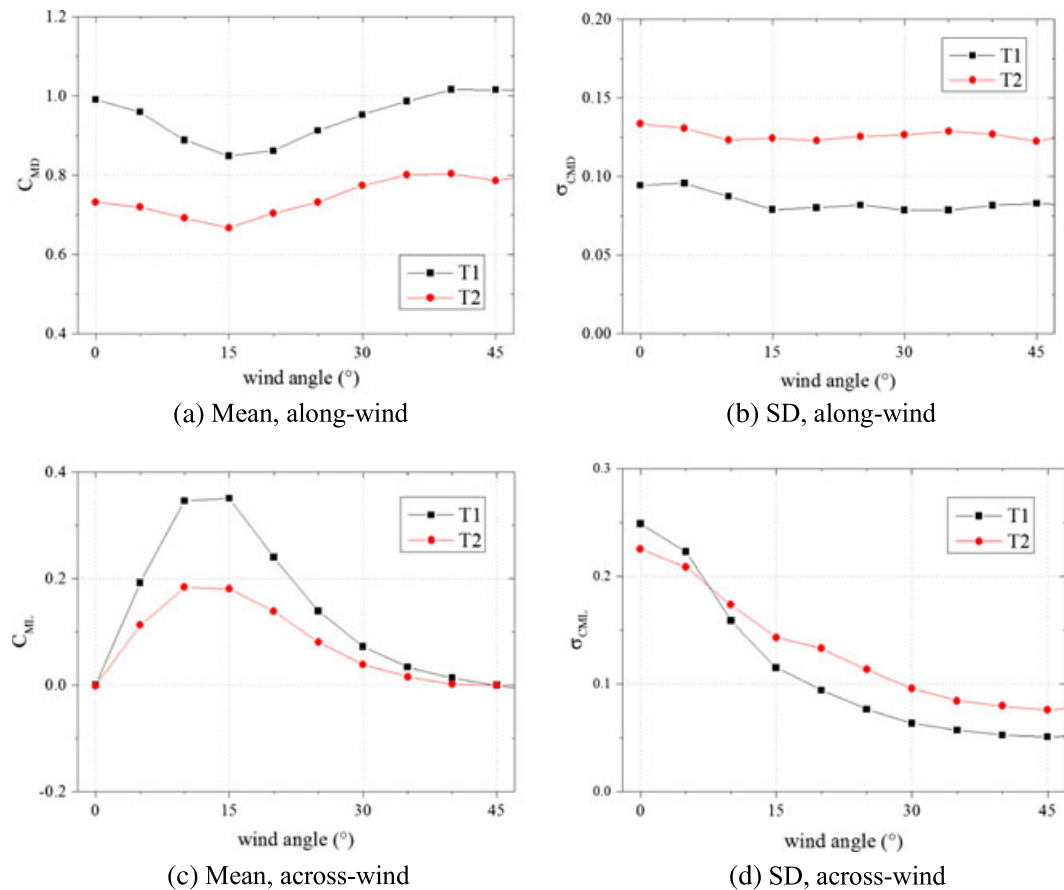


**FIGURE 24** Overturning moment coefficients (Model III, typhoon). SD = standard deviation

about twice the dominant reduced frequency of the across-wind load; this aspect deserves special consideration with reference to its potential contribution to the acceleration of the upper modes of vibration of super-tall buildings.

### 4.2 | Typhoon climate

The overturning moment coefficients of Model III in wind flows T1 and T2 are shown in Figure 24. The corresponding PSDs are shown in Figure 25.

The turbulence intensity in the wind flow T1 is smaller than that of T2 as may be noted from Figure 6. The effects of the turbulence intensity on the wind load in the Typhoon climate flow can be considered the same as those in the monsoon climate flow, that is, the mean wind load decreases and the fluctuating wind load increases on increasing the turbulence intensity, both in the along-wind and across-wind directions.

In addition, the mechanism of the wind load seems to be very sensitive to the turbulence intensity. When the turbulence intensity increases, the plateaux in the PSD of the along-wind force disappears, that is, distortions get stronger, whereas the vortex shedding load in the across-wind direction becomes weaker and the Strouhal number becomes closer to 0.1.

### 4.3 | Vortex shedding and characteristic turbulence intensity

Figure 26 shows the PSDs of the overturning moment coefficients of Model III (1,000 m-high) at  $\alpha = 0^\circ$  (wind orthogonal to a building face) in all the different wind-flow conditions examined here (E1, E2, E3, E4, T1, T2) as a function of the reduced frequency. Table 11 provides a list of the corresponding characteristic turbulence intensities as defined in section 3.3.

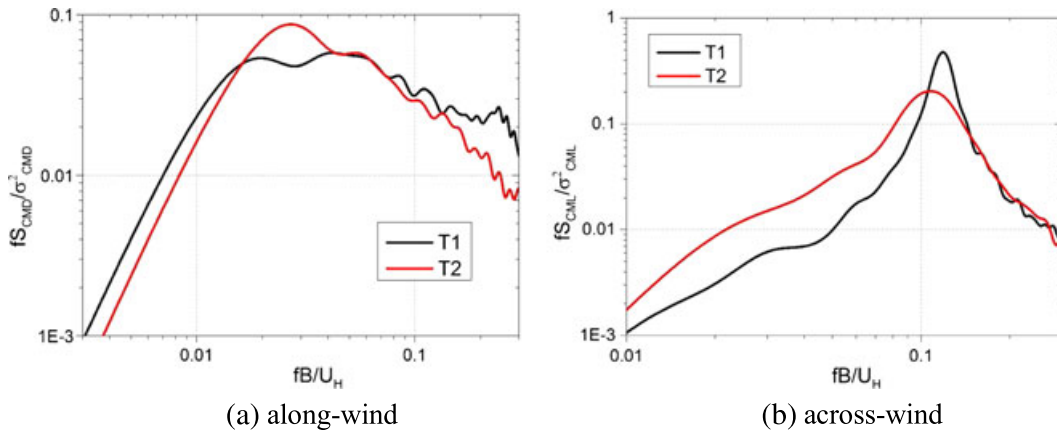


FIGURE 25 Power spectral density of the overturning moment coefficients (Model III,  $\alpha = 0^\circ$ , typhoon)

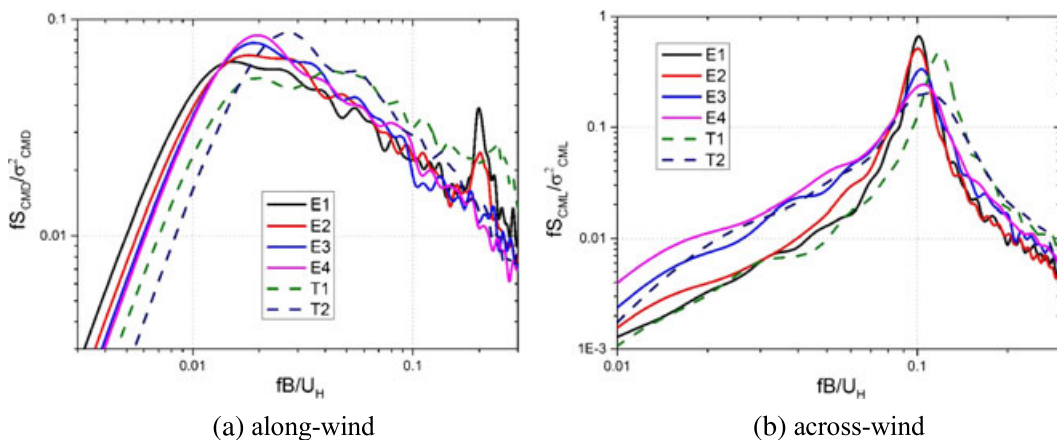


FIGURE 26 Power spectral density of the across-wind overturning moment coefficients (Model III,  $\alpha = 0^\circ$ )

**TABLE 11** Characteristic turbulence intensity

Model III	E1	E2	E3	E4	T1	T2
(1,000 m high)	7.74%	9.62%	12.26%	14.52%	9.88%	15.30%

It is apparent that the vortex shedding excitation closely depends on this parameter. When the characteristic turbulence intensity is lower than 10% (E1, E2, and T1), the vortex shedding is relevant in the long-wind direction at twice the critical reduced frequency in the across-wind direction. In addition, the characteristic turbulence intensity (in brackets) of the wind flows T1 (9.88%) and T2 (15.30%) are close to those of the wind flows E2 (9.62%) and E4 (14.52%), respectively. Accordingly, the shape and the peak value of the corresponding PSDs in the across-wind direction, as drawn from the wind flows T1 and T2, is similar to those drawn from the wind flows E2 and E4 (Figure 26).

## 5 | CONCLUSIONS AND PROSPECTS

The behavior of super-tall 1,000 m-high buildings under the action of strong winds is a big challenge in structural and wind engineering. This paper focuses on the aerodynamic wind load based on HFFB wind tunnel tests carried out at the Beijing Jiaotong University. The model suggested by Deaves and Harris is adopted as the target to simulate the wind flow of monsoon climate in the wind tunnel; four kinds of terrain roughness, that is, open (E1), countryside (E2), suburban (E3), and urban terrain (E4), are considered. In addition, the hurricane wind profile suggested by Vickery and Powell is adopted as the target to carry out preliminary simulations of the wind flow of typhoon climate; two levels of turbulence intensity are considered (T1 and T2).

HFFB tests for buildings 600 m (I), 800 m (II), 1,000 m (III), 1200 m (IV), and 1500 m (V) high are conducted to investigate the effects of building height on wind load. The results show that the aerodynamic load mainly depends on the wind flow. When the height is close to 1,000 m, the change of wind flow, especially the turbulence intensity, should be carefully considered. Smaller turbulence intensity leads to more intense vortex shedding, causing increasingly stronger structural excitation in the across-wind direction.

In order to better explain this situation, a new parameter is herein introduced, the characteristic turbulence intensity  $I_{char}$ , aiming to interpret and quantify the vortex shedding excitation. Smaller  $I_{char}$  values give rise to more intense vortex shedding and stronger structural excitation in the across-wind direction. It is worth noting that, on increasing the building height, the parameter  $I_{char}$  decreases in the typical monsoon climate (wind flow E3) but increases in the typical typhoon climate (wind flow T1).

It is also worth mentioning, however, the appearing of a significant vortex shedding excitation in the along-wind direction at twice the critical reduced frequency in the across-wind direction. In addition, the Strouhal number does not remain 0.1, but it changes from 0.12 to 0.14 as the wind direction changes from  $0^\circ$  to  $20^\circ$ ; this behavior seems to be apparent especially when the building height is beyond the inflection point of the mean wind speed profile. These aspects deserve further investigations.

The results provided by the present paper open the doors to new researches at least in two main directions.

The first research direction derives from the importance of the wind flow on the wind load. In this paper, target literature models have been used to simulate monsoon and typhoon wind-flow conditions in the wind tunnel. The models used, however, derive from studies that mainly focus, as it is usual, on wind-flow conditions close to the terrain. In order to improve the reliability of the studies addressed to super-tall buildings, it is thus crucial to carry out new field monitoring campaigns aiming to detect the wind field in the outer boundary layer, possibly up to the gradient height for monsoons and well above the inflection point for typhoons. This call for the use of new generation instruments such as the Radar Doppler<sup>[53]</sup> and the Lidar.<sup>[30,54]</sup>

The second research direction refers to the wind-excited and aeroelastic behavior of super-tall buildings subjected to the varied wind flow and wind-load conditions described in the present paper. Several items discussed herein let us argue the occurrence of structural motions and internal forces definitely changed with respect to traditional buildings. In this new framework, especially the aeroelastic performance of 1,000 m-high super-tall building is a key issue for further studies. It can be estimated that the fundamental frequency of 1,000 m-high super-tall buildings will be close to 0.07–0.08 Hz with aspect ratios at least 8–10. So, according to classic studies based on aeroelastic sectional models<sup>[55–58]</sup> and aeroelastic vibration tests on tall buildings models,<sup>[8–10,59,60]</sup> vortex-induced vibration, galloping, and vortex-induced vibration-

galloping interaction phenomena may occur, which is the new challenge. It is thus urgent to investigate all the possible forms of aeroelastic vibrations of super-tall buildings. A new research is in progress aiming to conduct a wide campaign of aeroelastic wind-tunnel tests. Within this framework, the issues related to the suppression of the vibrations through passive and active control systems are another key challenge.

Finally, it should be pointed out again that structural control must be used in 1,000 m-high building in order to satisfy their safe and comfortable requires at the acting of wind, especially in across-wind direction. Except traditional aerodynamic treatments used in wind engineering, passive, active, or semiactive structural control device is needed.<sup>[61–63]</sup> Furthermore, there are many innovative studies of health monitoring in high-rise buildings<sup>[64–66]</sup>; 1,000 m-high super-tall buildings is another important change to apply these techniques.

## ACKNOWLEDGEMENTS

This study is sponsored by the National Natural Science Foundation of China (51378060, 91215302) and the 111 Project of China (B13002).

## REFERENCES

- [1] <http://skyscrapercenter.com>
- [2] <http://www.buildingstructure.com.cn>
- [3] P. A. Irwin, *J. Wind Eng. Ind. Aerodyn.* **2009**, 97(7–8), 328.
- [4] G. Solari, *J. Eng. Mech.* **1985**, 111(2), 254.
- [5] A. Kareem, *J. Struct. Eng.* **1985**, 111, 2479.
- [6] A. Kareem, *J. Wind Eng. Ind. Aerodyn.* **1990**, 36, 589.
- [7] A. Kareem, *J. Wind Eng. Ind. Aerodyn.* **1992**, 41–44, 1101.
- [8] H. Kawai, *J. Wind Eng. Ind. Aerodyn.* **1992**, 41–44, 117.
- [9] H. Kawai, *J. Wind Eng. Ind. Aerodyn.* **1995**, 54–55, 125.
- [10] Kawai H. Vortex induced vibration, galloping and torsional flutter of tall buildings. The first international conference on advances in structural engineering and mechanics 1999, Seoul, Korea.
- [11] G. Solari, L. C. Pagnini, G. Piccardo, *J. Wind Eng. Ind. Aerodyn.* **1997**, 69, 719.
- [12] G. Piccardo, G. Solari, *J. Wind Eng. Ind. Aerodyn.* **1998**, 74–76, 697.
- [13] M. P. Repetto, G. Solari, *J. Wind Eng. Ind. Aerodyn.* **2004**, 92, 335.
- [14] X. Z. Chen, A. Kareem, *J. Eng. Mech.* **2005**, 131, 1115.
- [15] Y. Tamura, A. Kareem, G. Solari, K. C. S. Kwok, J. D. Holmes, W. H. Melbourne, *Wind Struct.* **2005**, 8(4), 251.
- [16] M. F. Huang, C. M. Chan, K. C. S. Kwok, P. A. Hitchcock, *J. Eng. Mech.* **2010**, 135(8), 802.
- [17] A. Kareem, *Wind Struct.* **1999**, 2(3), 201.
- [18] L. S. Fur, H. T. Y. Yang, S. Ankireddi, *J. Struct. Eng.* **1996**, 122(8), 948.
- [19] A. Ghosh, B. Basu, *Struct. Control Health Monit.* **2007**, 14(4), 681.
- [20] I. Venanzi, F. Ubertini, A. L. Materazzi, *Struct. Control Health Monit.* **2013**, 20(6), 903.
- [21] Y. Q. Ni, Z. G. Ying, J. Y. Wang, J. Ko, B. F. Spencer, *Probab. Eng. Mech.* **2004**, 19(3), 269.
- [22] H. Tanaka, Y. Tamura, K. Ohtake, *J. Wind Eng. Ind. Aerodyn.* **2012**, 107–108, 179.
- [23] E. K. Bandi, Y. Tamura, A. Yoshida, *J. Wind Eng. Ind. Aerodyn.* **2013**, 122, 60.
- [24] H. Tanaka, Y. Tamura, K. Ohtake, *Int. J. High-Rise Buildings* **2013**, 2(3), 213.
- [25] B. J. Vickery, *J. Fluid Mech.* **1966**, 25(3), 481.
- [26] AIJ-RLB-2004. Recommendations for loads on buildings. Architecture Institute of Japan 2004; Tokyo.
- [27] ASCE 7–10. Minimum design loads for buildings and other structures. Reston, VA, ASCE 2010; New York.
- [28] GB50009–2012. Load code for the design of building structures. China Architecture and Building Press 2012; Beijing.
- [29] Eurocode 1. Actions on structures – part 1-4: general actions – wind actions. European Committee for Standardisation 2005; Brussels.
- [30] A. Sathe, J. Mann, *Atmos. Meas. Tech.* **2013**, 6, 3147.
- [31] P. J. Vickery, D. Wadhwa, M. D. Powell, *J. Appl. Meteorol. Climatol.* **2009**, 48(2), 381.

- [32] P. J. Vickery, F. J. Masters, M. D. Powell, *J. Wind Eng. Ind. Aerodyn.* **2009**, 97(7), 392.
- [33] K. T. Tse, S. W. Li, P. W. Chan, *J. Wind Eng. Ind. Aerodyn.* **2013**, 115, 93.
- [34] L. L. Song, Q. S. Li, W. H. Chen, *Acta. Meteor. Sin.* **2005**, 63(6), 915.
- [35] S. Y. Cao, Y. Tamura, N. Kikuchi, *J. Wind Eng. Ind. Aerodyn.* **2009**, 97, 11.
- [36] B. Li, X. C. Zhang, Q. S. Yang, *J. Building Struct.* **2015**, 36(4), 99.
- [37] T. Tschanz, A. G. Davenport, *J. Wind Eng. Ind. Aerodyn.* **1983**, 13, 429.
- [38] J. Xie, P. A. Irwin, *J. Wind Eng. Ind. Aerodyn.* **1998**, 77-78, 579.
- [39] Deaves DM, Harris RI. A Mathematical model of the structure of strong winds. CIRIA Report 76; **1978**.
- [40] A. K. Blackadar, H. Tennekes, *J. Atmos. Sci.* **1968**, 25(6), 1015.
- [41] G. Solari, G. Piccardo, *Probab. Eng. Mech.* **2001**, 16(1), 73.
- [42] G. Solari, F. Tubino, *Probab. Eng. Mech.* **2002**, 17, 327.
- [43] D. M. Deaves, R. I. Harris, *Atmos. Environ.* **1982**, 16(8), 1889.
- [44] ESDU 82026. Strong winds in the atmospheric boundary layer. Engineering Sciences Data Unit 2002; London.
- [45] ISO 4354: 2009. Wind action on structures. The International Organization for Standardization 2009; Geneva.
- [46] RWDI. Wind tunnel test reports of Z15 tower. **2012**
- [47] Teunissen HW. Characteristics of the mean and turbulence in the planetary boundary layer. **1970**, UTIAS Review, No. 32.
- [48] Katsuchi H, Yamada H. . The 13th International Conference of Wind Engineering, **2011**, , *Netherland*.
- [49] J. D. Kepert, *J. Atmos. Sci.* **2001**, 58(17), 2469.
- [50] H. W. Tieleman, R. E. Akins, *J. Wind Eng. Ind. Aerodyn.* **1990**, 36, 579.
- [51] P. A. Irwin, *J. Wind Eng. Ind. Aerodyn.* **2008**, 96, 701.
- [52] ASCE-SEI 49-12. Wind tunnel testing for building's and other structures. American Society of Civil Engineers 2012; Virginia
- [53] W. S. Gunter, J. L. Schroeder, *J. Wind Eng. Ind. Aerodyn.* **2015**, 138, 13.
- [54] A. Sathe, J. Mann, N. Vasiljevic, *Atmos. Meas. Tech.* **2015**, 8, 729.
- [55] G. V. Parkinson, J. D. Smith, *Q. J. Mech. Appl. Math.* **1964**, 17(2), 225.
- [56] M. Novak, A. G. Davenport, *J. Eng. Mech. Div.* **1970**, 96(EM1), 17.
- [57] T. Sarpkaya, *J. Fluids Struct.* **2004**, 19, 389.
- [58] G. Piccardo, L. Carassale, A. Freda, *J. Wind Eng. Ind. Aerodyn.* **2011**, 99, 748.
- [59] M. Matsumoto, H. Ishizaki, C. Matsuoka, Y. Daito, Y. Ichikawa, A. Shimahara, *J. Wind Eng. Ind. Aerodyn.* **1998**, 77-78, 531.
- [60] C. M. Cheng, P. C. Lu, M. S. Tsai, *J. Wind Eng. Ind. Aerodyn.* **2002**, 90, 1743.
- [61] T. Tani, S. Yoshitomi, M. Tsuji, I. Takewaki, *Struct. Des. Tall Special Build.* **2009**, 18(7), 705.
- [62] K. A. Bani-hani, *Struct. Control Health Monit.* **2007**, 14(1), 83.
- [63] Y. Ikeda, *Struct. Control Health Monit.* **2009**, 16(7-8), 703.
- [64] T. H. Yi, H. N. Li, M. Gu, *Struct. Control Health Monit.* **2013**, 20(5), 649.
- [65] E. M. Hernandez, D. Bernal, L. Caracoglia, *Struct. Control Health Monit.* **2013**, 20(10), 1291.
- [66] Q. S. Li, L. H. Zhi, J. Yi, To A, J. Xie, *Struct. Control Health Monit.* **2014**, 21(6), 926.

**How to cite this article:** Li B, Yang Q, Solari G, Wu D. Investigation of wind load on 1,000 m-high super-tall buildings based on HFFB tests. *Struct Control Health Monit.* 2017;e2068. <https://doi.org/10.1002/stc.2068>